Periodic patterns in a ring of delay-coupled oscillators and spiking neurons

P. Perlikowski[1,2] and S. Yanchuk[1]

[1] *Institute of Mathematics, Humboldt University of Berlin, 10099, Berlin, Germany*

[2] *Division of Dynamics, Technical University of Lodz, 90-924 Lodz, Poland.*

O.V. Popovych[3] and P.A. Tass[3,4]

[3] *Institute of Neurosciences and Medicine - Neuromodulation (INM-7), Research Center Jülich, 52425 Jülich, Germany*

[4] *Department of Stereotaxic and Functional Neurosurgery, University Hospital, 50924 Cologne, Germany*

We describe the appearance and stability of spatio-temporal periodic patterns (rotating waves) in unidirectional rings of coupled oscillators with delayed couplings. We show how delays in the coupling lead to a splitting of each rotating wave into several new ones. The appearance of rotating waves is mediated by Hopf bifurcations of the symmetric equilibrium. We also conclude that the coupling delays can be effectively replaced by increasing the number of oscillators in the chain. The phenomena are shown for Stuart-Landau oscillators as well as for coupled FitzHugh-Nagumo systems interacting via excitatory chemical synapses.

I. INTRODUCTION

Networks of coupled dynamical systems [1] have become important models for studying the behavior of large complex systems. Such models allow to investigate fundamental features of coupled systems of different kinds, ranging from neurons to lasers, from living organisms to climate systems [2–5]. Various types of collective behavior have been found and well understood including synchronization [6] and desynchronization [7], clustering [8–10], multistabilities of high degree [11–13], etc.

In many realistic systems time delay effects play an important role due to a finite signal propagation time between different elements of the network. This is the case, for example, in systems of coupled semiconductor lasers [14–21], neuronal networks [22–25], biological oscillators [26], etc. Already for a few coupled systems time delays impose challenging problems [14, 16, 19, 27–29]. New phenomena emerge due to inclusion of time delays in complex networks [30–33].

This paper is devoted to the study of a delay coupled ring of oscillators shown schematically in Fig. 1. Systems with ring coupling are relevant for many practical situations [26, 34] and attracted a lot of attention in the past [10, 13, 35–45]. In particular, the existence and stability of phase-locked patterns and amplitude death states in bidirectionally coupled ring of oscillators have been studied in [42]. Chaotic rotating waves have been reported in [43, 46, 47]. Transient oscillations have been investigated in [48, 49]. Spatiotemporal patterns in rings of unidirectionally coupled oscillators have been analyzed in [13, 35, 50–52]. It is shown [13, 53] that at the transition from stationary to oscillatory behavior the network undergoes a complicated bifurcation scenario including the coexistence of multiple periodic orbits with different frequencies, spatial patterns, and modulation instabilities. The equation governing the dynamics of a network of delay-coupled oscillators near a multiple Hopf bifurcation is reduced to an amplitude-phase model without delay in [35] using the center manifold reduction and the normal form method. In the reduced model, the existence of traveling waves, in-phase and anti-phase locked oscillations is proved. Bifurcating periodic orbits in a unidirectional ring of three neurons with delays has been studied in [50]. The coexistence of stable periodic orbits in neural ring networks has been reported in [51].

Ensembles of unidirectionally coupled oscillators with ring topology [Fig. 1] play an important role in the modelling of neuronal dynamics and information processing in the neuroscience and medicine. Such networks are involved in the generation of stable periodic motor commands by central pattern generator of the nervous system controlling rhythmic locomotion in animals [54]. A ring-type topology is also present in the sequential feed-forward neuronal projections of a cortico-striatal-basal ganglia-thalamo-cortical motor loop relevant to the

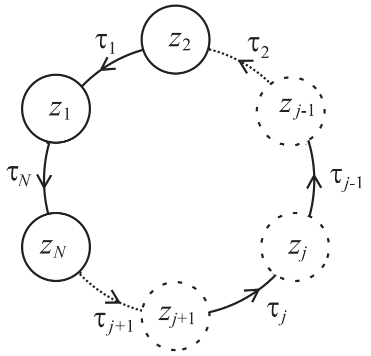

Figure 1: Scheme of coupling.

pathogenesis of Parkinson's disease [55]. A finite time delay in coupling naturally arises in such systems and, as we show below, might significantly influence the complexity of the collective dynamics by enhancing the multistability of synchronized spatio-temporal patterns.

We consider two models: a paradigmic model of coupled Stuart-Landau oscillators in the first part of the paper and a more realistic FitzHugh-Nagumo neuronal systems interacting via excitatory chemical synapses in the second part. The ring of delayed unidirectionally coupled dissipative Stuart-Landau oscillators [58] has the following form

$$\dot{z}_j(t) = (\alpha + i\beta)z_j(t) - z_j(t)\left|z_j(t)\right|^2 + z_{j+1}(t-\tau_j), \quad (1)$$

where $1 \leq j \leq N$, $z_j \in \mathbb{C}$ are complex variables for individual oscillators, α and β are real parameters, and $\tau_j > 0$ are time delays of the coupling (see Fig. 1). The ring structure implies $z_1 \equiv z_{N+1}$. The purpose of this paper is to investigate the effect of the coupling delays on the dynamics. Apart from the natural control parameter of the individual dynamics α, the following important control parameters appear in this setup: the round trip time delay $T = \tau_1 + \tau_2 + \cdots + \tau_N$ and the number of oscillators N in the ring. In particular, the cases with large number of oscillators N or/and large round trip delay T are investigated in detail.

In this paper, we describe the appearance and stability of spatio-temporal periodic patterns (rotating waves), which emerge from the symmetric equilibrium $z_1 = \cdots = z_N$ as a control parameter is changed. These patterns are similar to those appearing in systems without delay, which were reported in [13, 35, 36]. We show how the inclusion of additional delays τ_j in the coupling leads to the splitting of each rotating wave into several new ones. The appearance of rotating waves is mediated by Hopf bifurcations of the origin, whose frequency is independent on T and N. Moreover, the whole family of rotating waves have very a similar description in any of the following asymptotic cases: large number of oscillators N, large round trip time T, or both. We conclude that the coupling delays can effectively be replaced by increasing the number of oscillators in the chain N. In particular, the rotating waves as well as their stability in a ring of few oscillators (or even one oscillator with a delayed feedback) have similar properties as the rotating waves in a ring of N oscillators without delay provided N is sufficiently large.

The paper is organized as follows: In Sec. II we study the stability and spectrum of the symmetric equilibrium with respect to the control parameters α, T, and N. In Sec. III, we study the appearance of multiple periodic patterns as the equilibrium is destabilized through the Hopf bifurcations. In Sec. III B, we study the stability of these patterns and analyze the cases with large round trip time T or large number of oscillators N. In Sec. IV we consider a system of unidirectionally coupled FitzHugh-Nagumo (FHN) oscillators [59, 60] interacting via excitatory chemical synapses and demonstrate that the phenomena observed in the previous sections for coupled Stuart-Landau limit-cycle oscillators can be found for a ring of delay-coupled spiking neurons. Final conclusions are presented in Sec. V.

II. STABILITY AND SPECTRUM OF THE SYMMETRIC EQUILIBRIUM

Before proceeding to the analysis of the model, let us note that the delays in the coupling can be assumed to be identical without loss of generality. Indeed, given any distribution of delays $\tau_1, \tau_2, \ldots, \tau_N$, the following change of variables [53] $v_N(t) = z_N(t)$, $v_{N-1}(t) = z_{N-1}(t-(\tau - \tau_{N-1}))$, $v_{N-2}(t) = z_{N-2}(t-(2\tau - \tau_{N-1} - \tau_{N-2}))$, $\ldots$, $v_1(t) = z_1(t-(\tau_N - \tau))$ with $\tau = T/N$ leads to the same system as (1) but with identical time delays τ with respect to $v_j(t)$. Therefore we assume in the following that $\tau_j = \tau = T/N$.

A. Properties of the spectrum

The symmetric equilibrium at the origin $z_1 = \cdots = z_N = 0$ plays an important role in the development of the non-stationary dynamics in system (1). In particular, as we show in Sec. III, periodic patterns emerge from this equilibrium as some bifurcation parameter is varied, similarly to [13]. In order to study the corresponding bifurcations, in this section we investigate the eigenvalues of this equilibrium.

The stability of the origin can be studied by linearizing (1)

$$\dot{z}_j(t) = (\alpha + i\beta)z_j(t) + z_{j+1}(t-\tau). \tag{2}$$

The linearized system (2) can be diagonalized using the methods described in [13, 61]. As a result of such a diagonalization, instead of one high-dimensional coupled system (2) we obtain a set of N uncoupled systems of lower dimension. Formally, it can be achieved by the following discrete Fourier transformation $z_j(t) = \sum_{l=1}^{N} e^{i\varphi_l j} w_l(t)$, where $\varphi_l = 2\pi l/N$. Applying this transformation to system (2), we obtain the following set of independent systems

$$w_l'(t) = (\alpha + i\beta)w_l(t) + e^{i\varphi_l} w_l(t-\tau), \quad 1 \le l \le N. \tag{3}$$

Obviously, (3) determines the stability of the coupling mode φ_l, $1 \le l \le N$. The stability of each of these modes can be studied by the following characteristic equation

$$\lambda = (\alpha + i\beta) + e^{i\varphi_l - \lambda\tau}, \tag{4}$$

which is obtained by the substitution $w_l(t) = e^{\lambda t} w_{0l}$. Note, the characteristic equations for different coupling modes φ_l differ only by the phase factor $e^{i\varphi_l}$. If the number of oscillators is large, the values of φ_l densely fill the interval from 0 to 2π and one can approximate the phase φ_l by some continuous parameter $0 \le \varphi \le 2\pi$. Due to this fact we omit the index l below.

$$\lambda = (\alpha + i\beta) + e^{i\varphi - \lambda\tau}. \tag{5}$$

Equation (5) can formally be solved using the Lambert function, see e.g. [62, 63]

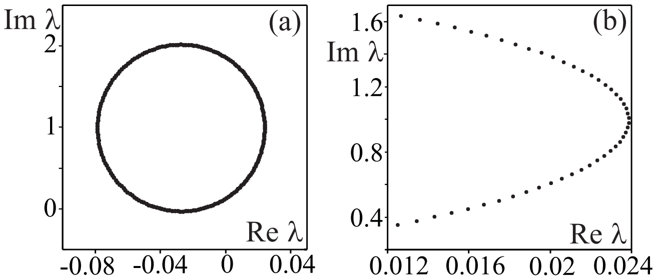

Figure 2: Spectrum of the origin in the array of delay coupled $N = 200$ oscillators. The round trip time is $T = 10$, which corresponds to a small delay $\tau = 0.05$ between the neighboring oscillators. The spectrum is approximated by the expression (7). (a) Whole spectrum; (b) zoom of the eigenvalues with the largest real parts. $\alpha = -0.99, \beta = 1$.

$$\lambda = \Lambda_\tau(\varphi) = (\alpha + i\beta) + \frac{1}{\tau} W\left(\tau e^{i\varphi - (\alpha+i\beta)\tau}\right). \tag{6}$$

The following asymptotic cases can be studied analytically:

Case 1. The interaction delay between oscillators is small $\tau \ll 1$.

Case 2. The interaction delay between oscillators is larger than the other characteristic time scales.

In the first case, one can neglect the delay and obtain the following set of eigenvalues

$$\Lambda_0(\varphi) = (\alpha + i\beta) + e^{i\varphi}, \;\; \varphi = \varphi_l, \, 1 \le l \le N, \tag{7}$$

which coincides with the spectrum for the ring of coupled oscillators without delay [13] [Fig. 2].

The situation becomes more complicated as the delay T increases. In particular, for each fixed coupling mode φ_l, an infinite number of additional eigenvalues become relevant, which can be associated with the "delay modes". For large delay, the pseudo-continuous spectrum approach [32, 63, 64] can be used. In order to obtain an approximation for the spectrum in this case, one should formally substitute $\lambda = i\omega + \gamma/\tau$ in the characteristic equation (5). As a first order approximation, we obtain the equation

$$i\omega = (\alpha + i\beta) + e^{-\gamma + i(\varphi - \omega\tau)},$$

which can be solved with respect to $\gamma(\omega)$

$$\gamma(\omega) = -\frac{1}{2}\ln\left(\alpha^2 + (\beta - \omega)^2\right).$$

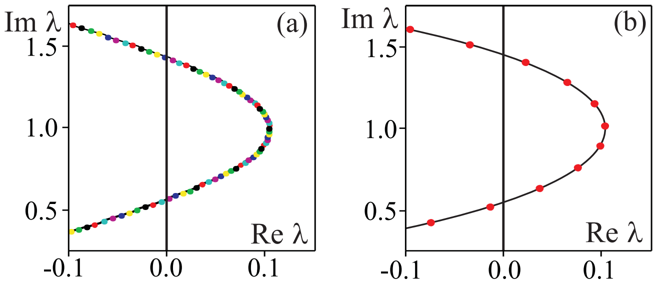

Figure 3: Spectrum of eigenvalues for $N = 7$ delay coupled Stuart-Landau oscillators with the round trip delay time $T = 350$. (a) Eigenvalues, associated with different coupling modes $\varphi_l = \frac{2\pi}{N} l$ (see (4)) are shown in different colors; (b) only the spectrum for the mode φ_1 is shown. Other parameters: $\alpha = -0.99$, $\beta = 1$. Color on-line.

The set of eigenvalues for large delay can be approximated by the following continuous curve [32, 63, 64]

$$\lambda = \Lambda_{\tau \gg 1}(\omega) = \frac{\gamma(\omega)}{\tau} + i\omega, \tag{8}$$

which is parametrized by ω. It is important to observe that the curve $\Lambda_{\tau\gg1}(\omega)$ does not depend on the coupling mode φ. This implies that the spectrum has the same asymptotic representation (8) for all coupling modes φ_l. As a result, the stability of each coupling mode is the same for sufficiently large delay. Figure 3(a) illustrates the whole spectrum of the eigenvalues and Fig. 3(b) shows only the eigenvalues, which are associated with one coupling mode. Even though the actual spectrum is discrete, the curve (8) gives a reasonable approximation, since the distances between the neighboring points of the spectrum is known [32, 64] to be small and proportional to $1/(\tau N)$.

Finally note that in the case $\alpha > 0$ and large τ, a strongly unstable eigenvalue exists [32, 63], which is close to $\alpha + i\beta$. This makes the system already unstable for all $\alpha > 0$, and no interesting bifurcation scenarios occur.

B. Conditions for Hopf bifurcations and Hopf frequencies

The destabilization of the symmetric equilibrium occurs through Hopf bifurcations. The condition for the Hopf bifurcations can be obtained by substituting $\Lambda = i\Omega_H$ into the characteristic equation

$$i\Omega_H = (\alpha + i\beta) + e^{i\varphi - i\Omega_H \tau}, \tag{9}$$

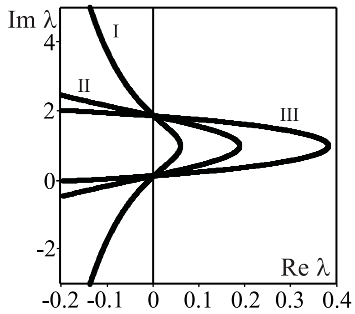

Figure 4: A part of the spectrum, corresponding to the eigenvalues with the largest real parts (critical eigenvalues). The spectrum (I) corresponds to $N = 100$, (II) to $N = 500$ and (III) to $N = 3000$. Although the eigenvalues come closer to the imaginary axis and scale as $1/\tau$ with an increase of $\tau = T/N$, the spectrum crosses the imaginary axis at the same Hopf points $i\Omega_H$. The other parameters read $\alpha = -0.99$, $\beta = 1$, $T = 1000$ and are fixed.

where Ω_H is the Hopf frequency. The equation (9) can be solved with respect to the Hopf frequency

$$(\Omega_H - \beta)^2 + \alpha^2 = 1 \tag{10}$$

or

$$\Omega_H = \beta \pm \sqrt{1 - \alpha^2} \tag{11}$$

after excluding the unknown phase argument $\varphi - \Omega_H \tau$. Expression (11) shows that the Hopf frequencies are independent of the number N of oscillators and the delay τ for given parameters of individual oscillators α and β.

Note the asymptotic approximations (7) and (8) of the spectrum preserve this property. More precisely, the Hopf frequencies, which can be obtained from the approximated spectra (7) and (8) coincide with the exact frequencies given by (10).

The illustration in Fig. 4 shows the spectra for different values of N with some fixed α, β, and T. One can observe that all spectra cross the imaginary axis at the same Hopf points $i\Omega_H$ as it is predicted by the theory. The additional effect is that the eigenvalues come closer to the imaginary axis as the delay τ increases and their real part scales as $1/\tau$ [see (8)]. Yet this effect does not influence neither the Hopf frequency nor the destabilization threshold.

Figure 5 illustrates how the whole spectrum changes as the number of oscillators is changed. More precisely,

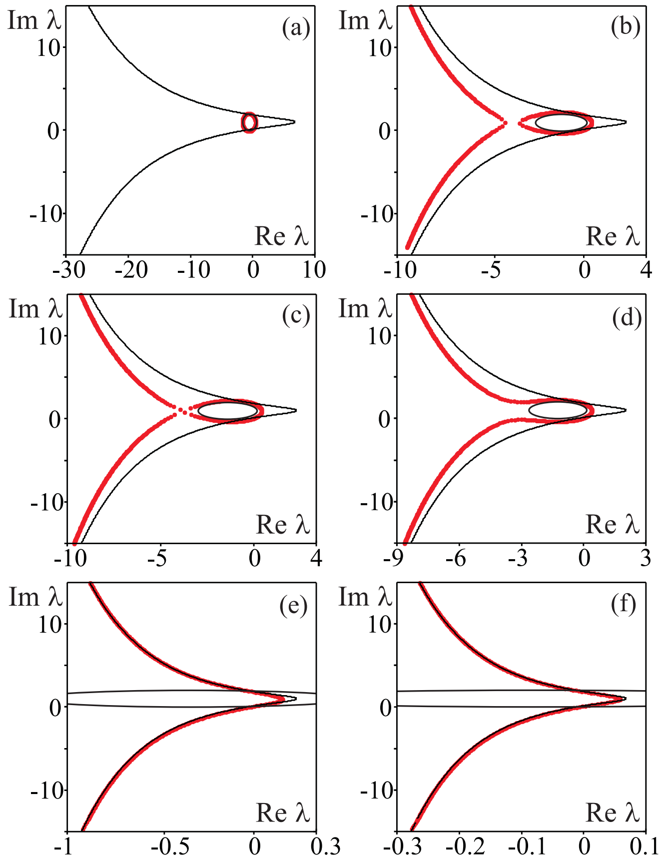

Figure 5: Change of the spectrum as N is changed with fixed round trip T. The spectrum [bold red points] continuously transforms from the typical lattice spectrum in (a) to the typical large delay spectrum in (f). Parameter values: $\alpha = -0.5$, $\beta = 1$, $T = 100$ and $N = 1000$ (a), $N = 320$ (b), $N = 318$ (c), $N = 300$ (d), $N = 30$ (e) $N = 10$ (f). Thin black lines show the positions of the asymptotic spectra (7) and (8) for large N and large T limits.

the parameters $\alpha = -0.5$, $\beta = 1$, $T = 100$ are fixed, and N is decreased from 1000 to 10 (this corresponds to an increase of τ from 0.1 to 10). As the number of oscillators decreases, the spectrum transforms from that shown in [Fig. 5(a)], which is typical for lattices of coupled oscillators without delay, to the spectrum shown in [Fig. 5(f)], which is typical for systems with large delay.

C. Hopf curves and stability domains with respect to parameters

In the case when the number of oscillators or delay time is large, the conditions for stability of the origin can be written using the asymptotic spectra. More exactly, in the case of large N and small delay, the stability condition is $\mathrm{Re}\left[\Lambda_0(\varphi)\right] < 0$, i.e.

$$\mathrm{Re}\left[(\alpha + i\beta) + e^{i\varphi}\right] < 0, \quad 0 \le \varphi \le 2\pi,$$

while in the case of a large delay τ (N can attain any positive integer value), the stability condition is $\mathrm{Re}\left[\Lambda_{\tau\gg1}(\omega)\right] < 0$, i.e.

$$\mathrm{Re}\left[\frac{\gamma(\omega)}{\tau} + i\omega\right] < 0, \quad \omega \in \mathbb{R}.$$

It is remarkable that both cases yield the same stability condition

$$\alpha < -1.$$

This simple condition holds as soon as N is large or τ is large. In the case when N or τ admits intermediate values, the stability of the origin can still be achieved for $\alpha > -1$. The explanation for this effect is the following: although the continuous asymptotic spectra (8) and (7) are unstable for $\alpha > -1$, the positions of the eigenvalues on the spectral lines may "miss" the unstable parts of the curves [see similarly in [63]].

Let us consider the exact characteristic equation (5) and obtain the curves of Hopf bifurcations in the parameter space. From the Hopf condition (9) we obtain

$$\arg(-\alpha - i\beta + i\Omega_H) = \varphi - \Omega_H \tau_H.$$

Taking into account that $\varphi = \varphi_l = 2\pi l/N$ and $\tau = T/N$ we obtain

$$\arg(-\alpha - i\beta + i\Omega_H) = \frac{2\pi l}{N} - \Omega_H \frac{T}{N}$$

Let us choose N and T to be our control parameters. Then the representation for the lines of Hopf bifurcations in the parametric plane (N, T) reads

$$N = \frac{2\pi l - \Omega_H T}{\arg(-\alpha - i\beta + i\Omega_H)}, \quad l = 0, \pm1, \pm2, \ldots. \tag{12}$$

Here Ω_H is given by (11). Figure 6 shows a two-parameter diagram for $\alpha = 0.99$ and $\beta = 1$, where the Hopf bifurcation lines are shown. The shaded ares in the bifurcation diagram denote the domains where the origin is stable. The boundary of this domain denotes the first

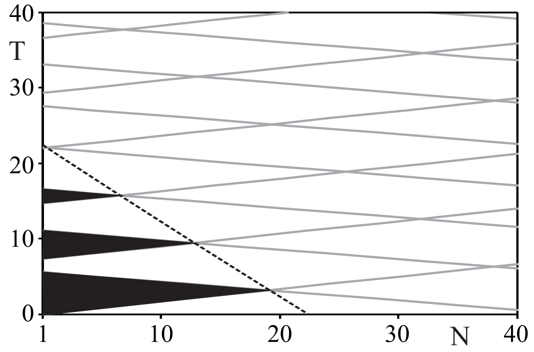

Figure 6: Hopf bifurcation curves are shown in gray. The origin is stable for the parameter values from the black areas. The dashed black line is the stability boundary given by (15). $\alpha = -0.99, \beta = 1$.

Hopf bifurcation, which leads to the initial destabilization of the origin.

As predicted by the theory, the domains of stability disappear as T or N increase. Such a size limitation can be estimated quantitatively by finding the line in the parameter space, which connects the peaks of the stability domains [see Fig. 6]. Each peak of the stability domain corresponds to the parameter value, for which a double Hopf bifurcation occurs. The condition for the double Hopf bifurcation is given by

$$i\Omega_{H1} = (\alpha + i\beta) + e^{i\varphi_1 - i\Omega_{H1}\tau}, \tag{13}$$

$$i\Omega_{H2} = (\alpha + i\beta) + e^{i\varphi_2 - i\Omega_{H2}\tau}, \tag{14}$$

where $\Omega_{H1,2} = -\beta \pm \sqrt{1-\alpha^2}$ and $\varphi_1 - \varphi_2 = \frac{2\pi}{N}$. If we denote $\chi(\alpha) = \arg(-\alpha + i\sqrt{1-\alpha^2})$, we obtain from (13) and (14)

$$\varphi_2 + \frac{2\pi}{N} - \beta\tau - \sqrt{1-\alpha^2}\tau = \chi(\alpha),$$

$$\varphi_2 - \beta\tau + \sqrt{1-\alpha^2}\tau = -\chi(\alpha).$$

Excluding φ_2 and substituting $\tau = \frac{T}{N}$, we obtain

$$\frac{2\pi}{N} - 2\sqrt{1-\alpha^2}\frac{T}{N} = 2\chi(\alpha),$$

from which we finally get

$$T\sqrt{1-\alpha^2} + \chi(\alpha)N = \pi. \tag{15}$$

The obtained Eq. (15) shows the boundary of the possible stability domain of the origin. As soon as $T\sqrt{1-\alpha^2} + \chi(\alpha)N > \pi$, a stabilization is not possible. Although the condition (15) is independent on β, exact positions of the stability domains [black regions in Fig. 6] do depend on the value of β.

III. EMERGING PERIODIC PATTERNS

In this section we describe emerging periodic solutions of system (1). We derive a relation between the number of the periodic solution branches and the coupling time delay τ. We show that these periodic solutions correspond to periodic patterns emerging with increasing N or/and τ. In the second part of this section we analyze the stability of the periodic solutions (resp. patterns) and compare different cases: coupled oscillators without delay, single oscillator with delay, and delayed coupled oscillators. The words "pattern" and "solution" are used interchangeably below, though the former one underlines the spatial structure and the latter one the fact that they are resulting from the dynamics of system (1).

A. Shape of periodic patterns

Due to the spatio-temporal symmetries, system (1) has periodic solutions in the form of rotating waves [similarly to [13]]:

$$z_j(t) = ae^{i\varphi_l j + i\omega t}, \tag{16}$$

where $\varphi_l = \frac{2\pi}{N}l$, a and ω are the unknown amplitude and frequency of the periodic solutions respectively. After substituting (16) to Eq. (1) we obtain the following equation

$$i\omega = \alpha + i\beta - a^2 + e^{i(\varphi_l - \omega\tau)}, \tag{17}$$

which leads to the following system

$$a = \sqrt{\alpha + \cos(\varphi_l - \omega\tau)}, \tag{18}$$

$$\omega = \beta + \sin(\varphi_l - \omega\tau) \tag{19}$$

for the amplitude and frequency of a periodic solution. Let us denote the solutions of (18) and (19) as a_{lk} and

ω_{lk}. We number now the solutions with two indices l and k, since for each fixed l, the equation (19) has multiple solutions, the number of which increases with the delay. >From equation (19) we see that $\beta - 1 \le \omega \le \beta + 1$.

Each periodic solution originates in a Hopf bifurcation (see Eq. (11)) of the symmetric equilibrium. The number of bifurcations grows with an increase of the number of oscillators as well as with increase of the time delay in the coupling. In Fig. 7(a,b) we show branches of periodic solutions for $N = 11$, $\tau = 0$ and $N = 1$, $\tau = 15$ versus control parameter α. In these two cases the number of periodic solutions is the same. In Fig. 7(c) we illustrate how the number of solutions of Eq. (19) is growing due to the increase of the time delay τ in the given range of β (see Eq. (16)).

Figure 8 illustrates the spatio-temporal structure of different patterns. The upper part of the figure shows the patterns, which correspond to the coupling modes with $l = 0, \pm 1$ and small delay. With an increase of the delay, each pattern gives rise to multiple additional delay induced patterns (numbered by k) as illustrated in the lower figure for $l = 0$.

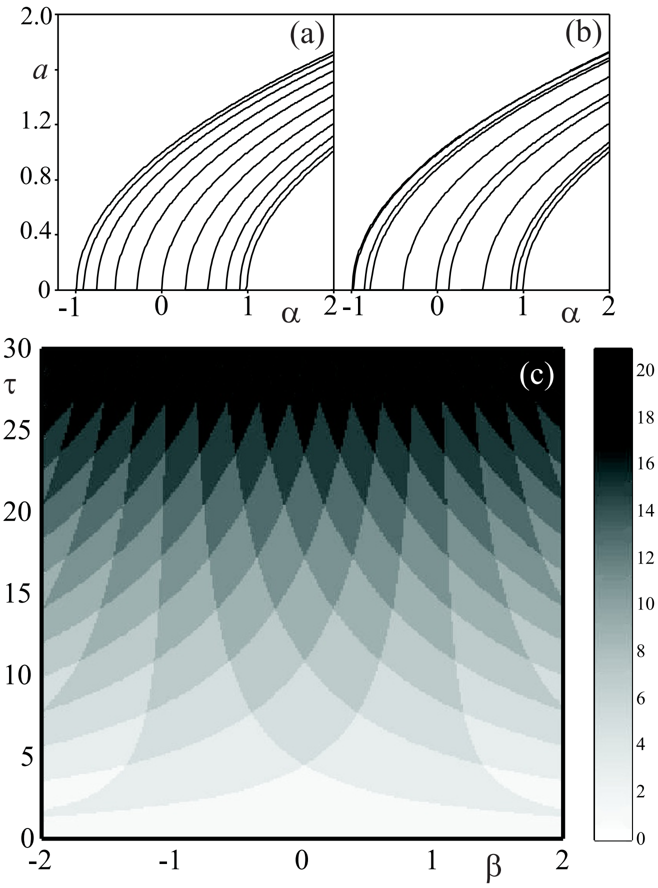

Figure 7: Families of periodic solutions for (a) ring of $N = 11$ coupled oscillators without delay [see Eq. (16)] and (b) a single delayed oscillator with $\tau = 15$ [see Eq. (23)]. The same number of branches is present in both cases. In (c) the number of periodic solutions is shown in gray as a function of two parameters: β and the time delay τ for a single oscillator with the delayed feedback.

B. Stability of patterns

The stability of the obtained periodic patterns can be described by the spectrum of Floquet multipliers. Even though the main purpose of this paper is to study the ring of delay-coupled oscillators, in what follows we compare three cases: a single oscillator with delayed feedback, a ring of unidirectionally coupled oscillators without time delay, and a ring of unidirectionally delay-coupled systems. We will show some remarkable similarities of the families of periodic solutions in all three cases, but also important differences.

In order to determine the stability of the periodic patterns (16), one has to linearize the equations of motion (1) around the corresponding solutions. Before doing such a linearization, let us transform system (16) with the following change of coordinates (i.e., a co-rotating frame)

$$z_j(t) = a_{lk} e^{i\varphi_l j + i\omega_{lk} t}(x_j(t) + iy_j(t)),$$

where x_j and y_j are new real coordinates. With respect to the new coordinates, the system has the following form

$$\begin{aligned} x_j' &= \left(a_{lk}^2 - \cos\chi_{lk}\right) x_j - y_j \sin\chi_{lk} - a_{lk}^2 x_j (x_j^2 + y_j^2) \\ &\quad + x_{j+1}(t-\tau)\cos\chi - y_{j+1}(t-\tau)\sin\chi_{lk}, \end{aligned}$$

$$\begin{aligned} y_j' &= -x_j \sin\chi_{lk} + \left(a_k^2 - \cos\chi_{lk}\right) y_j - a_{lk}^2 y_j (x_j^2 + y_j^2) \\ &\quad + x_{j+1}(t-\tau)\sin\chi_{lk} + y_{j+1}(t-\tau)\cos\chi_{lk} \end{aligned}$$

and the periodic solution (16) is transformed into the family of equilibria $x_j + iy_j = e^{i\kappa}$, $\kappa \in \mathbb{R}$. Here we denote $\chi_{lk} = \varphi_l - \tau\omega_{lk}$. In order to find its stability, it is necessary to linearize around any of this equilibria, since all of them have the same stability properties. We choose $x_j = y_j = 1/\sqrt{2}$. The corresponding linearized system

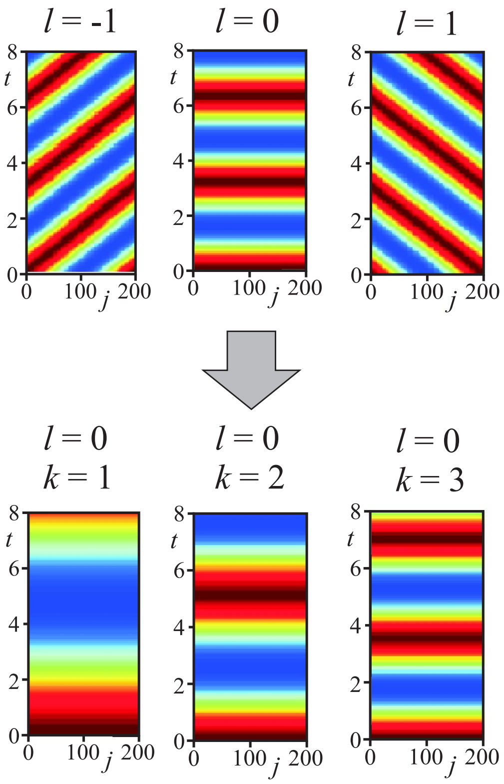

Figure 8: Spatio-temporal patterns for some of the bifurcating time-periodic solutions (16) corresponding to different values of l (coupling modes). In (a,b,c) we show patterns in a ring of coupled oscillators where a particular value of l corresponds to a single frequency ω_{l1} and an amplitude a_{l1}. As the delay increases, new frequencies ω_{01}, ω_{02}, and ω_{03} appear (as well as ω_{l1},ω_{l2}, ...), which correspond to additional delay modes. The lower panel illustrates new delay induced patterns for $l = 0$ and $\tau = 10$. (see also Fig. 7c). $\alpha = -0.5, N = 200, \beta = 1$.

reads in vector form

$$\begin{bmatrix} \delta x'_j \\ \delta y'_j \end{bmatrix} = -\left(C_{lk} + a_{lk}^2 \begin{bmatrix} 1 & 1 \\ 1 & 1 \end{bmatrix}\right) \begin{bmatrix} \delta x_j \\ \delta y_j \end{bmatrix} + C_{lk} \begin{bmatrix} \delta x_{j+1}(t-\tau) \\ \delta y_{j+1}(t-\tau) \end{bmatrix}, \qquad (20)$$

where

$$C_{lk} = \begin{bmatrix} \cos\chi_{lk} & -\sin\chi_{lk} \\ \sin\chi_{lk} & \cos\chi_{lk} \end{bmatrix}.$$

System (20) can be uncoupled (diagonalized) in a similar way as we have done it with the system (2), namely, by applying the transformation $[\delta x_j, \delta y_j]^T = \sum_{m=1}^{N} e^{i\varphi_m j} [\delta u_m, \delta y_m]^T$ with $\varphi_m = 2\pi m/N$, $m = 1, \ldots, N$. As a result, we obtain the uncoupled system

$$\begin{bmatrix} \delta u'_m \\ \delta u'_m \end{bmatrix} = -\left(C_{lk} + a_{lk}^2 \begin{bmatrix} 1 & 1 \\ 1 & 1 \end{bmatrix}\right) \begin{bmatrix} \delta u_m \\ \delta v_m \end{bmatrix} + e^{i\varphi_m} C_{lk} \begin{bmatrix} \delta u_m(t-\tau) \\ \delta v_m(t-\tau) \end{bmatrix},$$

which leads to the following characteristic equation

$$\det\left[\mu I + a_{lk}^2 \begin{bmatrix} 1 & 1 \\ 1 & 1 \end{bmatrix} + C_{lk}\left(1 - e^{i\varphi_m - \mu\tau}\right)\right] = 0$$

or, equivalently,

$$0 = \mu^2 + 2\mu\left(a_{lk}^2 + \left(1 - e^{i\varphi_m - \mu\tau}\right)\cos\left(\varphi_l - \tau\omega_{lk}\right)\right) \qquad (21)$$
$$+2a_{lk}^2\left(1 - e^{i\varphi_m - \mu\tau}\right)\cos\left(\varphi_l - \tau\omega_{lk}\right) + \left(1 - e^{i\varphi_m - \mu\tau}\right)^2.$$

The solutions μ of this characteristic equation determine the stability of the periodic solution. Let us recall that all periodic solutions, which we consider, are characterized by the two indexes l and k. The index $1 \le l \le N$ stands for the coupling modes and k for the additional delay modes. Thus, by fixing some k and l, one fixes a particular periodic pattern [see also Fig. 8]. The index m stands for the different perturbation modes, i.e. solutions of (21) for all different $1 \le m \le N$ constitute a set of eigenvalues μ determining the stability of a given pattern. In particular, if all the eigenvalues have negative real parts (except for the trivial one, which is zero and corresponds to the Floquet multiplier 1), then the chosen pattern is asymptotically stable.

C. Characterizing stable and unstable patterns

In this section we provide an analysis of the stability of the periodic patterns using the derived characteristic equation (21) and comparing it with the known cases of a single oscillator with delay and coupled oscillators without delay [13, 32]. In the Appendix, we derive the characteristic equation for periodic solutions (rotating waves) for the single Stuart-Landau oscillator with delayed feedback of the form

$$\dot{z}(t) = (\alpha + i\beta)z(t) - z(t)\left|z(t)\right|^2 + z(t-\tau). \qquad (22)$$

Such periodic solutions have the form

$$z(t) = a_k e^{i\omega_k t} \qquad (23)$$

with some amplitude a_k and frequency ω_k given by (31) and (32). Their stability is governed by the characteristic equation (see Appendix)

$$0=\mu^2+2\mu\left(a_k^2+\left(1-e^{-\mu\tau}\right)\cos\left(\omega_k\tau\right)\right) \qquad (24)$$
$$+2a_k^2\left(1-e^{-\mu\tau}\right)\cos\left(\omega_k\tau\right)+\left(1-e^{-\mu\tau}\right)^2=0.$$

In the ring of coupled Stuart-Landau oscillators without delay [13]

$$\dot{z_j}(t)=(\alpha+i\beta)z_j(t)-z_j(t)\left|z_j(t)\right|^2+z_{j+1}(t) \qquad (25)$$

the corresponding periodic patterns take the form (16). Contrary to the delayed case, the amplitude and frequency are explicitly given by $a_l=\sqrt{\alpha+\cos\varphi_l}$ and $\omega_l=\beta+\sin\varphi_l$. Their stability is described by the polynomial characteristic equation

$$0=\mu^2+2\mu\left(a_l^2+\left(1-e^{i\varphi_m}\right)\cos\varphi_l\right) \qquad (26)$$
$$+2a_l^2\left(1-e^{i\varphi_m}\right)\cos\varphi_l+\left(1-e^{i\varphi_m}\right)^2.$$

It is easy to see that the characteristic equation for the ring of delayed coupled oscillators (21) is generalization of two cases (24) and (26). Moreover, as we will see below, the asymptotic cases, where either the delay or the number of oscillators is large, provide the same result concerning the existence and stability of the periodic patterns in all three cases.

Let us start with the Hopf bifurcation condition, where the periodic patterns lose their stability. The Hopf bifurcation condition can be obtained by substituting $\mu=i\Omega$ into the characteristic equation. As a result, we obtain the following conditions:
Case 1 (single delayed oscillator):

$$0=-\Omega^2+2i\Omega\left(a_k^2+\left(1-e^{-i\Omega\tau}\right)\cos\chi_d\right)$$
$$+2a_k^2\left(1-e^{-i\Omega\tau}\right)\cos\chi_d+\left(1-e^{-i\Omega\tau}\right)^2. \qquad (27)$$

Case 2 (coupled oscillators without delay):

$$0=-\Omega^2+2i\Omega\left(a_l^2+\left(1-e^{i\varphi_m}\right)\cos\chi_c\right)$$
$$+2a_l^2\left(1-e^{i\varphi_m}\right)\cos\chi_c+\left(1-e^{i\varphi_m}\right)^2. \qquad (28)$$

Case 3 (delayed coupled oscillators):

$$0=-\Omega^2+2i\Omega\left(a_{lk}^2+\left(1-e^{i\varphi_m-i\Omega\tau}\right)\cos\chi_{cd}\right)$$
$$+2a_{lk}^2\left(1-e^{i\varphi_m-i\Omega\tau}\right)\cos\chi_{cd}+\left(1-e^{i\varphi_m-i\Omega\tau}\right)^2 (29)$$

where $\varphi_m=2\pi m/N$, $1\le m\le N$, and the numbers l and k characterize the chosen pattern. Here we denoted by $\chi_d=\omega_k\tau$, $\chi_c=\varphi_l$, and $\chi_{cd}=\varphi_l-\tau\omega_{lk}$ the quantities, which have the same meaning in all cases, i.e. the relative phase differences between neighboring oscillators also taking into account the delay. Now it is easy to see that the only difference between the equations (27), (28), and (29) is the phase factor in the exponents. In the case, when the number of oscillators N is large or the delay τ is large, this factor does not influence the Hopf frequency, since φ_m covers the whole phase range from 0 to 2π. In particular, it implies that the asymptotic spectrum crosses the imaginary axis at the same Hopf frequencies in all three cases. This, in turn, implies that, intriguingly, the stability properties of the periodic patterns in all three cases are the same.

Thus, we draw here the following important conclusion from the stability analysis: The periodic rotating waves in three different cases (1), (22), and (25) have the same asymptotic stability properties, i.e. if any two patterns are characterized by the same (or nearly the same) phase difference χ between neighboring oscillators taking into account also the time delay shift, then they are either stable or unstable simultaneously. In the case of the single oscillator, χ is just a phase shift due to the delay.

As a result, for the stability of the family of patterns (16) one can immediately obtain the Eckhaus bifurcation scenario [13, 65]. This scenario is illustrated in Fig. 9. There we compare the families of periodic solutions for the above mentioned three cases. The amplitude a (i.e. a_l or a_k, or a_{kl} correspondingly) of solutions is plotted versus parameter α. The black line denotes a boundary between stable and unstable periodic solutions (in solid and dotted gray lines respectively). In particular, all solutions above this line are asymptotically stable, and the solutions below the line are unstable. Obviously, the Eckhaus line is the same for all cases, while the family of periodic solutions may contain different numbers of solutions depending on the delay or the size of the array N. Finally, we note that the rate of multistability is increased in comparison with the non-delayed case due to the interaction delays.

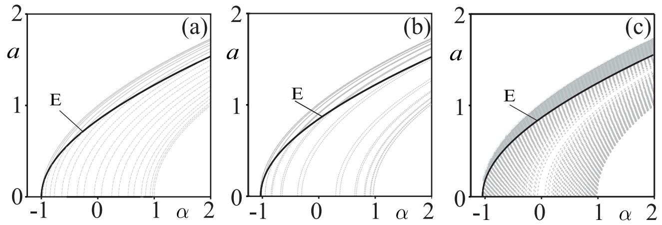

Figure 9: Periodic patterns and their stability for (a) twenty coupled systems without delay, (b) one system with delayed feedback with $\tau = 15$ and (c) twenty delayed coupled oscillators with $\tau = 15$. The solid black line in each plot shows the stability boundary (above this line periodic solutions are stable).

IV. COUPLED SPIKING NEURONS

In this section we demonstrate that the phenomena observed in the previous sections for coupled Stuart-Landau limit-cycle oscillators can be found for a ring of delay-coupled spiking neurons. We consider a system of unidirectionally coupled FitzHugh-Nagumo (FHN) oscillators [59, 60] interacting via excitatory chemical synapses

$$\begin{aligned}
\dot{v}_j &= v_j - v_j^3/3 - w_j + I_j + C(V - v_j)s_{j+1}(t-\tau), \\
\dot{w}_j &= 0.08(v_j + 0.7 - 0.8w_j), \qquad (30) \\
\dot{s}_j &= 0.5(1 - s_j)/(1 + \exp(-4(v_j - 1.5))) - 0.6s_j, \\
& \qquad j = 1, 2, \ldots, N.
\end{aligned}$$

Variable v_j models the membrane potential of a single cell, and I_j is a constant current controlling the spiking dynamics of a neuron. In what follows we consider I_j being randomly Gaussian distributed around the mean value $\overline{I} = 0.4$ with standard deviation $\sigma = 0.005$. For such values of I_j the time-averaged spiking frequencies f_j (average number of spikes per second) of individual neurons are distributed around the mean frequency $\overline{f} \approx 23.6$Hz with standard deviation $\sigma_f \approx 0.13$ [Fig. 10(a), black dots]. The synaptic coupling between the neurons in ensemble (30) is realized via a post-synaptic potential s_j generated by neuron j [66, 67]. It is modeled in the standard way by an additional equation for $s_j(t)$ [68, 69]. Parameter C defines the coupling strength, τ is the time delay in coupling, and V is the reversal potential taken as $V = 2$ for excitatory coupling. As for the ensemble of Stuart-Landau limit-cycle oscillators (1), we assume that the neurons are unidirectionally coupled in a ring such that $s_{N+1} \equiv s_1$.

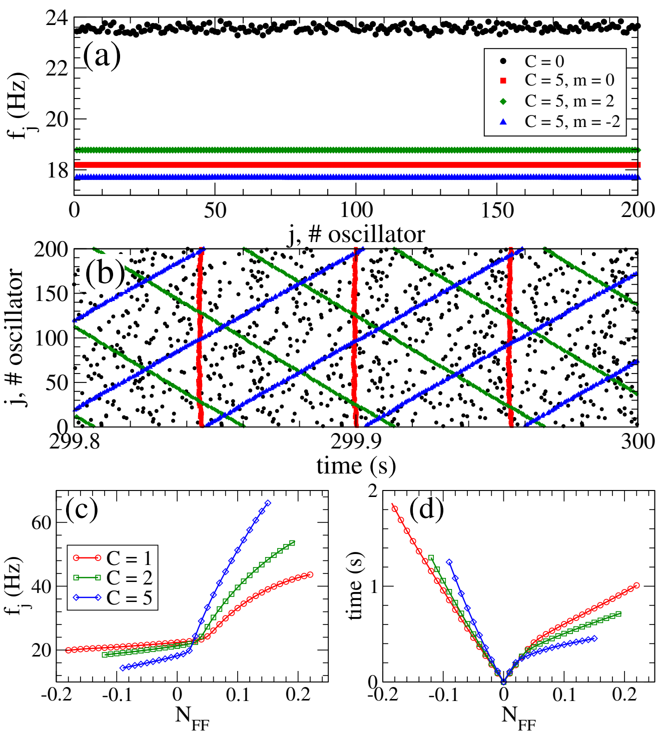

Figure 10: Synchronized spatial dynamics of the unidirectionally synaptically coupled spiking neurons (30). (a) Individual time-averaged spiking frequencies f_j (average number of spikes per second) for different initial conditions leading to different numbers of traveling firing fronts on the ring $m = 0$ (in-phase synchronization), $m = 2$, and $m = -2$ and coupling strength C as indicated in the legend. A negative value in the latter case means that the traveling fronts move in the direction opposite to the direction of coupling in the ensemble. (b) Raster plot of the neuronal firing, where the onsets of spikes are indicated by dots. The color of dots corresponds to that in plot (a), see legend. (c) Synchronized spiking frequencies of stable traveling m-front solutions versus the relative number $N_{FF} = m/N$ of the firing fronts. The coupling strength is indicated in the legend. (d) Traveling time of a complete rotation of the firing fronts along the ring of neurons. Same coloring as in plot (c). Number of oscillators $N = 200$ and delay $\tau = 0$.

We first consider the case of zero delay $\tau = 0$. If the coupling strength in the neuronal ensemble (30) increases, the neurons synchronize and oscillate with the same frequency [Fig. 10(a)]. Depending on the initial conditions the frequency of the synchronized states can attain different values indicating a multistability of synchronized regimes. For example, for narrowly distributed initial conditions $\{(v_j(0), w_j(0), s_j(0))\}_{j=1}^N$ the oscillators synchronize at the frequency $f_j \approx 18.2$Hz [Fig. 10(a), red dots], whereas for broadly distributed initial condition the synchronized frequency can be $f_j \approx 18.8$Hz or $f_j \approx 17.7$Hz [Fig. 10(a), green and blue dots]. To investigate this phenomenon we consider the above initial conditions distributed on a limit cycle $\gamma(t) = (v(t), w(t), s(t))$, $t \in [0, T]$ of a single FHN neuronal oscillator, where T is a period of oscillations. Following Eq. (16), for a fixed integer l the initial conditions are taken as $(v_j(0), w_j(0), s_j(0)) = \gamma(t_j)$, where $t_j = j\frac{T}{N}l \pmod T$. The above synchronized states with different synchronized frequencies are obtained for $l = 0, 2$, and -2.

Besides different frequencies, synchronized neurons demonstrate a different spatial organization of the spiking dynamics. For narrowly distributed initial conditions, e.g., for $l = 0$, the oscillators are in-phase synchronized and all neurons fire simultaneously [Fig. 10(b), red dots]. On the other hand, for broadly distributed initial conditions the neuronal activity can be organized in a traveling wave regime having one or several firing fronts traveling along the ring. In such a regime, the next neuron in the ring fires after its neighboring neuron generates a spike. Intriguingly, the firing fronts can move along the ring either in the direction of the synaptic coupling or in the opposite direction. For example, for $l = 2$ we obtain two traveling fronts propagating along the ring in the direction of the coupling [Fig. 10(b), green dots]. Conversely, for $l = -2$ the two traveling firing fronts move along the ring in opposite direction of the coupling [Fig. 10(b), blue dots]. We also note that uncoupled and desynchronized neurons do not demonstrate any spatial structure [Fig. 10(b), black dots].

We found that a number of m-front solutions can be stable for the neuronal ensemble (30) for a range of the firing fronts m [Fig. 10(c),(d)]. For the traveling front dynamics we define the relative number of the firing fronts $N_{FF} = m/N$, where the number of traveling fronts m can be either positive or negative depending on whether the fronts travel along or against the direction of the coupling, respectively. Each of such solutions is characterized by different synchronized spiking frequency $f_j = f$, which increases if the number of positive fronts (positive m) increases and decreases for increasing number of negative fronts (negative m) [Fig. 10(c)]. Furthermore, the spatial velocity of the front propagation along the network significantly slows down if the number of firing fronts (either positive or negative) increases. It is also worth noting that a stronger coupling in the neuronal ensemble (30) without delay appears to counteract the stability of the firing fronts and makes the range of the stable fronts smaller [Fig. 10(c),(d)]. These results agree with those obtained for the relaxation oscillators, like the Morris-Lecar and the Ellias-Grossberg neuronal models, where strong coupling among neurons supports the in-phase synchronization at the expenses of the traveling waves [70].

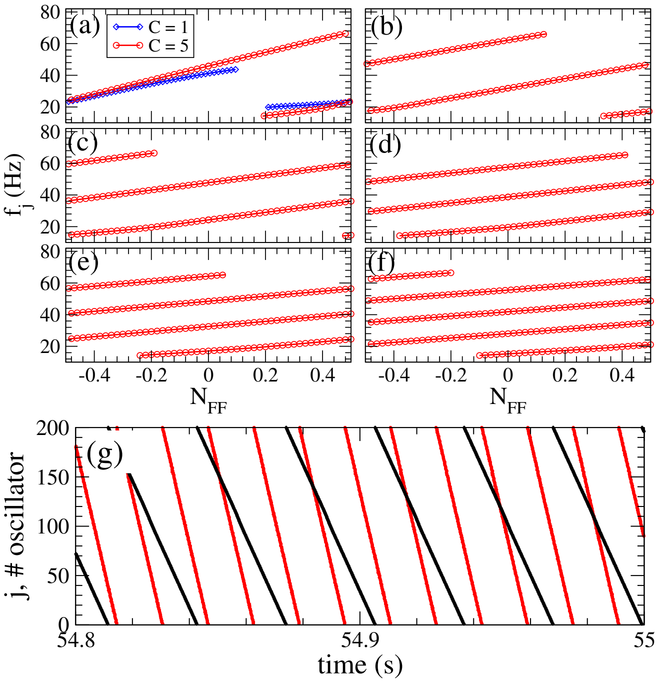

Figure 11: Delay-induced multistability of the traveling firing fronts of the unidirectionally synaptically coupled spiking neurons (30). (a)-(f) Individual time-averaged spiking frequencies f_j (average number of spikes per second) versus the relative number $N_{FF} = m/N$ of the firing fronts for different coupling strength C in (a) as indicated in the legend and delay (a) $\tau = 20$ms, (b) 30ms, (c) 40ms, (d) 50ms, (e) 60 ms, and (f) 70ms. (g) Raster plot of the neuronal firing, where the onsets of spikes are indicated by dots. For different initial conditions two different coexisting stable solutions can be found (black and red dots) of $m = 1$ traveling firing fronts. Delay $\tau = 30$ms and the coupling strength $C = 5$, which corresponds to plot (b). Coupling $C = 5$ in (b)-(f), and the number of oscillators (a)-(c) $N = 200$ and (d)-(f) $N = 100$.

The situation is different for a finite delay τ in the coupling between the neurons. Stronger coupling apparently promotes the stability of the traveling firing fronts and extends the range of stable fronts [Fig. 11(a)]. For large delay and coupling the neuronal ensemble (30) exhibits multistability of the traveling firing fronts, which becomes more pronounced if the time delay gets larger [Fig. 11(b)-(f)]. In such a way, several stable m-front solutions with the same number m of the firing fronts can coexist. They differ from each other by the spiking frequencies f_j of the synchronized neurons and, correspondingly, by the propagation time on the ring. For example, for delay $\tau = 30$ms and coupling $C = 5$, and for the range of the relative number of traveling fronts $N_{FF} \in [-0.5, 0.135] \cup [0.335, 0.5]$ system (30) has two stable m-front solutions with the same number $m = N_{FF}N$ (for $N = 200$, $m \in [-100, 27] \cup [67, 100]$) of the firing fronts but with different spiking frequencies f_j of synchronized neurons [Fig. 11(b)]. For the above values of the parameters, the two different stable m-front solutions with $m = 1$ firing fronts are illustrated in Fig. 11(g) [red and black dots]. The number of coexisting stable m-front solutions with the same number $m = N_{FF}N$ of the firing fronts increases as the time delay in system (30) gets larger. For example, there exist three different stable m-front solutions for delay $\tau = 40$ms, 50ms [Fig. 11(c),(d)], four different stable m-front solutions for delay $\tau = 60$ms, 70ms [Fig. 11(e),(f)], and so on.

The delay-induced multistability of the in-phase synchronized states ($m = 0$ traveling firing fronts) of the neuronal ensemble (30) [Fig. 10(b), red dots] can be investigated with the help of a single neuron with delayed feedback, i.e., for $N = 1$ in Eq. (30). Indeed, since for small parameter mismatch among the neurons the in-phase synchronization is characterized by almost identical amplitude dynamics of the neurons, they could be replaced by a single neuron with delayed feedback. In this way, the continuation by delay parameter τ of a single neuron with delayed feedback reveals an interval of bistability of the spiking dynamics for $\tau \in (6.7, 10)$ and feedback strength $C = 5$ [Fig. 12(a), red curve]. In this parameter interval different initial conditions can lead to either slow [Fig. 12(a), red curve, lower branch] or fast [Fig. 12, red curve, upper branch] spiking dynamics of a neuron. For example, for $\tau = 7$ and $C = 5$, the FHN neuron with delayed feedback can oscillate with either

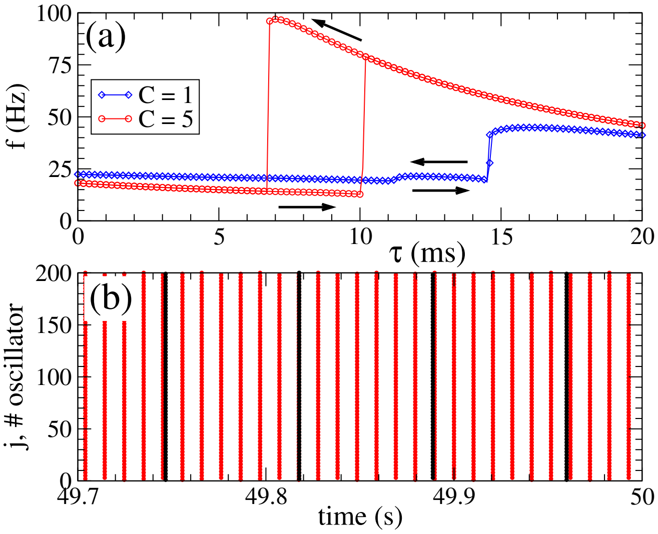

Figure 12: Delay-induced bistability of the in-phase synchronized states of the unidirectionally synaptically coupled spiking neurons (30). (a) Spiking frequency of a single FHN neuron with delayed feedback, i.e., $N = 1$ in system (30), versus time delay τ for the feedback strength C as indicated in the legend. The direction of continuation by parameter τ is indicated by arrows. (b) Raster plot of the neuronal firing, where the onsets of spikes are indicated by dots. Two stable coexisting in-phase synchronized states (black and red dots) of the ensemble of $N = 200$ identical spiking neurons (30) are illustrated for coupling $C = 5$ and delay $\tau = 7$ms. The constant currents $I_j = 0.4$.

$f = 14$Hz or $f = 96.9$Hz. This dynamics is reflected by a system of $N = 200$ identical FHN neurons (30), where the neuronal oscillators synchronize in-phase either at one or another of the above frequencies for a proper choice of the initial conditions [Fig. 12(b), black and red dots]. For a smaller feedback strength $C = 1$ the continuation by parameter τ in both directions gives the same values of the spiking frequency and a bistability region is not visible in the scale of the plot [Fig. 12(a), blue curve].

Although the multistability of the in-phase synchronized solutions of the neuronal ensemble (30) can be found for relatively small values of the time delay [Fig. 12], the "long-range" multistability of the traveling firing fronts starts at larger delays [Fig. 11]. It is interesting to observe that the spiking frequencies f_j of the coexisting stable traveling-front solutions are bounded to some frequency interval $f_j \in [f_{\min}, f_{\max}]$, which depends on the coupling strength and can be found already for the delay-free case, i.e. for $\tau = 0$. Indeed, the spiking frequencies of the stable m-front solutions of neurons (30) coupled without delay ($\tau = 0$) are bounded, for instance, to the interval $f_j \in [14\text{Hz}, 66\text{Hz}]$ for $C = 5$ and to the interval $f_j \in [20\text{Hz}, 44\text{Hz}]$ for $C = 1$ [Fig. 10(c)]. This property is preserved if a finite delay is introduced [Fig. 11(a)]. Then the multistability of the traveling-front solutions is manifested in that the branches of such solutions densely fill the above frequency intervals as the delay in the coupling between the neurons increases [Fig. 11(a)-(f)]. This is in accordance with the results obtained for the delay-coupled Stuart-Landau limit-cycle oscillators, see Eq. (19).

V. CONCLUSIONS

In summary, the introduction of delays in a ring of coupled oscillators leads to the emergence of additional rotating waves and their multistability. The emergence of rotating waves is mediated by Hopf bifurcations of the symmetric equilibrium. We have described stability properties of emerging periodic patterns. The phenomena are shown analytically for the Stuart-Landau oscillators as well as numerically for coupled FitzHugh-Nagumo systems interacting via excitatory chemical synapses. In order to obtain the analytical description of the phenomena, we have extensively used the phase-shift symmetry of the Stuart-Landau oscillators, i.e. the symmetry of the system with respect to the transformation $z \to e^{i\varphi}z$. This symmetry allows to obtain the explicit expressions for the rotating waves. The similarity of the results for the FitzHugh-Nagumo and Stuart-Landau systems indicate that the described phenomena do not depend on the explicit form or symmetries of the individual oscillator.

The results obtained in this study are also relevant from a neuroscientific standpoint. To reveal the directionality of interaction within loops of neurons or neuronal populations, experimentalists often infer the directionality of interaction from the sequence of activation or firing [e.g [56, 57]]: A sequential activation is typically interpreted as being caused by a directional coupling in the sense that neurons that fire later are driven by those which fire earlier. Our study nicely illustrates the rich and – from the classical experimentalist's standpoint – puzzling situation that the directionality of interaction need not at all correspond to the timing pattern of the units forming the loop. Although in our model there is a purely unidirectional coupling, the neurons may fire coincidently or they may fire one after the other in sequence, corresponding to the directionality of coupling. And, intriguingly, they may even fire in reverse order, i.e. in a timing sequence completely opposite to the directionality of coupling. This nicely illustrates that the standard procedure, used by experimentalists, to identify timing sequences with coupling patterns may actually lead to enormous artifacts.

Acknowledgments

P. P. and S. Y. acknowledge the support of DFG Research Center Matheon "Mathematics for key technologies" under the project D21. P.P. acknowledges the support of Department of International Co-operation of Poland under Project No. DWM/N97/DAAD/2008.

---

[1] S. H. Strogatz, Nature **410**, 268 (2001).
[2] R. Zillmer, R. Livi, A. Politi, and A. Torcini, Phys. Rev. E **74**, 036203 (2006).
[3] E. Mosekilde, Y. Maistrenko, and D. Postnov, *Chaotic Synchronization. Application to Living Systems.* (World Scientific, 2002).
[4] C. Hauptmann, O. Popovych, and P. A. Tass, Biol Cybern **93**, 463 (2005), URL `http://dx.doi.org/10.1007/s00422-005-0020-1`.
[5] A. Tsonis and P. Roebber, Physica A: Statistical and Theoretical Physics **333**, 497 (2004).
[6] A. Pikovsky, M. Rosenblum, and J. Kurths, *Synchronization. A Universal Concept in Nonlinear Sciences* (Cambridge University Press, 2001).
[7] P. A. Tass, *Phase Resetting in Medicine and Biology*, Stochastic Modelling and Data Analysis, Series: Springer Series in Synergetics (Springer, 1999).
[8] H. Daido and K. Nakanishi, Phys. Rev. E **75**, 056206 (pages 16) (2007), URL `http://link.aps.org/abstract/PRE/v75/e056206`.
[9] K. Kaneko, Physica D **41**, 137 (1990).
[10] S. Yanchuk, Y. Maistrenko, and E. Mosekilde, Math.

Comp. Simul **54**, 491 (2001).
[11] V. A. Makarov, E. del Río, W. Ebeling, and M. G. Velarde, Phys. Rev. E **64**, 036601 (2001).
[12] P. G. Lind, J. Corte-Real, and J. A. C. Gallas, Phys. Rev. E **69**, 066206 (pages 12) (2004), URL http://link.aps.org/abstract/PRE/v69/e066206.
[13] S. Yanchuk and M. Wolfrum, Phys. Rev. E **77**, 026212 (pages 7) (2008), URL http://link.aps.org/abstract/PRE/v77/e026212.
[14] H. Erzgräber, B. Krauskopf, and D. Lenstra, SIAM J. Appl. Dyn. Syst. **5**, 30 (2006).
[15] T. W. Carr, I. B. Schwartz, M.-Y. Kim, and R. Roy, SIAM J. Appl. Dyn. Syst. **5**, 699 (2006).
[16] O. D'Huys, R. Vicente, T. Erneux, J. Danckaert, and I. Fischer, Chaos **18**, 037116 (pages 11) (2008), URL http://link.aip.org/link/?CHA/18/037116/1.
[17] I. Fischer, R. Vicente, J. M. Buldú, M. Peil, C. R. Mirasso, M. C. Torrent, and J. Garcia-Ojalvo, Phys. Rev. Lett. **97**, 123902 (2006).
[18] T. Heil, I. Fischer, W. Elsäßer, J. Mulet, and C. R. Mirasso, Phys. Rev. Lett. **86**, 795 (2001).
[19] R. Vicente, I. Fischer, and C. R. Mirasso, Physical Review E (Statistical, Nonlinear, and Soft Matter Physics) **78**, 066202 (pages 11) (2008), URL http://link.aps.org/abstract/PRE/v78/e066202.
[20] H.-J. Wünsche, S. Bauer, J. Kreissl, O. Ushakov, N. Korneyev, F. Henneberger, E. Wille, H. Erzgräber, M. Peil, W. Elsäßer, et al., Phys. Rev. Lett. **94**, 163901 (2005).
[21] A. L. Franz, R. Roy, L. B. Shaw, and I. B. Schwartz, Phys. Rev. E **78**, 016208 (pages 19) (2008), URL http://link.aps.org/abstract/PRE/v78/e016208.
[22] C. Hauptmann, O. Omel'chenko, O. V. Popovych, Y. Maistrenko, and P. A. Tass, Phys Rev E Stat Nonlin Soft Matter Phys **76**, 066209 (2007).
[23] C. Masoller, M. C. Torrent, and J. Garcia-Ojalvo, Physical Review E (Statistical, Nonlinear, and Soft Matter Physics) **78**, 041907 (pages 8) (2008), URL http://link.aps.org/abstract/PRE/v78/e041907.
[24] E. Rossoni, Y. Chen, M. Ding, and J. Feng, Phys. Rev. E **71**, 061904 (2005).
[25] M. Dhamala, V. K. Jirsa, and M. Ding, Phys. Rev. Lett. **92**, 074174 (2004).
[26] A. Takamatsu, R. Tanaka, H. Yamada, T. Nakagaki, T. Fujii, and I. Endo, Phys. Rev. Lett **87**, 078102 (2001).
[27] H. G. Schuster and P. Wagner, Prog. Theor. Phys. **81**, 939 (1989).
[28] S. Yanchuk, Phys. Rev. E **72**, 036205 (2005).
[29] C.-U. Choe, T. Dahms, P. Hövel, and E. Schöll, Phys. Rev. E **81**, 025205 (2010).
[30] J. Kestler, W. Kinzel, and I. Kanter, Physical Review E (Statistical, Nonlinear, and Soft Matter Physics) **76**, 035202 (pages 4) (2007), URL http://link.aps.org/abstract/PRE/v76/e035202.
[31] M. G. Rosenblum, A. S. Pikovsky, and J. Kurths, Phys. Rev. Lett. **78**, 4193 (1997).
[32] M. Wolfrum and S. Yanchuk, Phys. Rev. Lett **96**, 220201 (2006).
[33] G. C. Sethia, A. Sen, and F. M. Atay, Physical Review Letters **100**, 144102 (pages 4) (2008), URL http://link.aps.org/abstract/PRL/v100/e144102.
[34] P. Woafo and H. G. E. Kadji, Phys. Rev. E **69**, 046206 (pages 9) (2004), URL http://link.aps.org/abstract/PRE/v69/e046206.
[35] M. Bonnin, Physica D: Nonlinear Phenomena **238**, 77 (2009), ISSN 0167-2789, URL http://www.sciencedirect.com/science/article/B6TVK-4TBXG99-1/2/32435f37f1571117b4681a00cd317c5e.
[36] W. Zou and M. Zhan, SIAM Journal on Applied Dynamical Systems **8**, 1324 (2009), URL http://link.aip.org/link/?SJA/8/1324/1.
[37] I. Waller and R. Kapral, Phys. Rev. A **30**, 2047 (1984).
[38] H. Daido, Phys. Rev. Lett. **78**, 1683 (1997).
[39] J. G. Restrepo, E. Ott, and B. R. Hunt, Phys. Rev. Lett. **93**, 114101 (pages 4) (2004), URL http://link.aps.org/abstract/PRL/v93/e114101.
[40] D. M. Abrams and S. H. Strogatz, Phys. Rev. Lett. **93**, 174102 (pages 4) (2004), URL http://link.aps.org/abstract/PRL/v93/e174102.
[41] P. C. Bressloff, S. Coombes, and B. de Souza, Phys. Rev. Lett. **79**, 2791 (1997).
[42] R. Dodla, A. Sen, and G. L. Johnston, Phys. Rev. E **69**, 056217 (2004).
[43] I. P. Marino, V. Pérez-Mu nuzuri, V. Pérez-Villar, E. Sánchez, and M. A. Matías, Phys. D **128**, 224 (1999), ISSN 0167-2789.
[44] G. V. der Sande, M. C. Soriano, I. Fischer, and C. R. Mirasso, Physical Review E (Statistical, Nonlinear, and Soft Matter Physics) **77**, 055202 (pages 4) (2008), URL http://link.aps.org/abstract/PRE/v77/e055202.
[45] Y. Zhang, G. Hu, and H. A. Cerdeira, Phys. Rev. E **64**, 037203 (2001).
[46] M. A. Matías and J. Güémez, Phys. Rev. Lett. **81**, 4124 (1998).
[47] X. L. Deng and H. B. Huang, Phys. Rev. E **65**, 055202 (2002).
[48] K. Pakdaman, C. P. Malta, C. Grotta-Ragazzo, O. Arino, and J.-F. Vibert, Phys. Rev. E **55**, 3234 (1997).

[49] Y. Horikawa and H. Kitajima, Physica D: Nonlinear Phenomena **238**, 216 (2009), ISSN 0167-2789, URL http://www.sciencedirect.com/science/article/B6TVK-4TGS79D-1/2/102ae643e825ce0e615f7acff7191653.

[50] S. J. Guo and L. H. Huang, Acta Mathematica Sinica, English Series **23**, 799 (2007).

[51] F. Pasemann, Neural Networks **8**, 421 (1995).

[52] P. Perlikowski, S. Yanchuk, M. Wolfrum, A. Stefanski, P. Mosiolek, and T. Kapitaniak, Chaos **20**, 013111 (2010).

[53] P. Baldi and A. Atia, IEEE Transactions on Neural Networks **5**, 1045 (1994).

[54] M. Golubitsky, I. Stewart, P.-L. Buono, and J. J. Collins, Nature **401**, 693 (1999).

[55] H. Bergman, A. Feingold, A. Nini, A. Raz, H. Slovin, M. Abeles, and E. Vaadia, Trends Neurosci. **21**, 32 (1998), ISSN 0166-2236, URL http://www.sciencedirect.com/science/article/B6T0V-3TGMNDF-W/2/2d2425991879a580c4ac9ab5fdf04437.

[56] J. Volkmann, M. Joliot, A. Mogilner, A. A. Ioannides, F. Lado, E. Fazzini, U. Ribary, and R. LlinÃ¡s, Neurology **46**, 1359 (1996).

[57] J. Gross, J. Kujala, M. Hamalainen, L. Timmermann, A. Schnitzler, and R. Salmelin, Proc Natl Acad Sci U S A **98**, 694 (2001), URL http://dx.doi.org/10.1073/pnas.98.2.694.

[58] Y. Kuramoto, *Chemical Oscillations, Waves, and Turbulence* (Springer, Berlin, 1984).

[59] R. FitzHugh, Biophys. J. **1**, 445 (1961).

[60] J. Nagumo, S. Arimoto, and S. Yoshizawa, Proc. IRE pp. 2061–2071 (1962).

[61] L. M. Pecora and T. L. Carroll, Phys. Rev. Lett. **80**, 2109 (1998).

[62] P. Hövel and E. Schöll, Phys. Rev. E **72**, 046203 (2005).

[63] S. Yanchuk, M. Wolfrum, P. Hövel, and E. Schöll, Phys. Rev. E **74**, 026201 (2006).

[64] M. Lichtner, M. Wolfrum, and S. Yanchuk, *The spectrum of delay differential equations with large delay*, Preprint 647. DFG Research Center Matheon, Strasse des 17 Juni 136, 10623 Berlin (Submitted to SIAM J. Math. Analysis) (2009), URL http://www.matheon.de/research/show_preprint.asp?action=details&serial=647.

[65] S. Yanchuk and M. Wolfrum, in *Proceedings of ENOC-2005*, edited by D. van Campen, M. Lazurko, and W. van der Oever (Eindhoven, Netherlands, 2005), pp. 1060–1065.

[66] W. Gerstner and W. M. Kistler, *Spiking neuron models: single neurons, populations, plasticity* (Cambridge Univ. Press, Cambridge, 2002).

[67] E. M. Izhikevich, *Dynamical systems in neuroscience: the geometry of excitability and bursting* (MIT Press, Cambridge, Mass., 2007).

[68] D. Golomb and J. Rinzel, Phys. Rev. E **48**, 4810 (1993).

[69] D. Terman, J. E. Rubin, A. C. Yew, and C. J. Wilson, Journal of Neuroscience **22**, 2963 (2002), http://www.jneurosci.org/cgi/reprint/22/7/2963.pdf, URL http://www.jneurosci.org/cgi/content/abstract/22/7/2963.

[70] D. Somers and N. Kopell, Biological Cybernetics **68**, 393 (1993).

VI. APPENDIX. CHARACTERISTIC EQUATION FOR ROTATING WAVES IN THE SINGLE STUART-LANDAU OSCILLATOR WITH DELAYED FEEDBACK

The equation for a single Stuart-Landau oscillator with delayed feedback is given by (22). Properties of the periodic patterns in this system have been considered in [32] in the limit of large delay by transforming it to the complex Ginzburg-Landau equation. Here we derive the corresponding characteristic equation directly for Eq. (22).

First of all, periodic solutions of Eq. (22) can be obtained by substituting

$$z(t) = ae^{i\omega t}$$

into (22). The resulting equations can be solved with respect to the amplitude and frequency:

$$a_k = \sqrt{\alpha + \cos\left(\omega_k \tau\right)}, \tag{31}$$

$$\omega_k = \beta - \sin\left(\omega_k \tau\right), \tag{32}$$

where index k corresponds to different solutions of the transcendental Eq. (32) for given τ, α, and β.

In order to find the stability of the obtained periodic solutions $a_k e^{i\omega_k t}$, we linearize the system (22) around these solutions. For this, we first make the transformation in (22) by introducing new variables $x\left(t\right)$ and $y\left(t\right)$

$$z\left(t\right) = a_k e^{i\omega_k t}\left(x\left(t\right) + iy\left(t\right)\right),$$

which leads to the following system with respect to $x(t)$ and $y(t)$

$$\begin{aligned}\dot{x}(t) &= \alpha x\left(t\right) - \left(\beta-\omega_k\right) y\left(t\right) - x\left(t\right)\left(x^2(t)+y^2(t)\right) \\ &\quad + x(t-\tau)\cos\left(\omega_k\tau\right) + y(t-\tau)\sin\left(\omega_k\tau\right), \\ \dot{y}(t) &= \alpha y\left(t\right) + \left(\beta-\omega_k\right) y\left(t\right) - y\left(t\right)\left(x^2(t)+y^2(t)\right) \\ &\quad - x(t-\tau)\sin\left(\omega_k\tau\right) + y(t-\tau)\cos\left(\omega_k\tau\right).\end{aligned} \tag{33}$$

In the new system, the periodic solution $z(t)=a_k e^{i\omega_k t}$ is reduced to the family of equilibria $x+iy=e^{i\kappa}$, $\kappa\in\mathbb{R}$. In order to find its stability, it is necessary to linearize (33) around any of this equilibria. We choose $x=y=1/\sqrt{2}$. The corresponding linearized system in the vector form reads as follows

$$\begin{aligned}\begin{bmatrix}\delta x'\left(t\right)\\ \delta y'\left(t\right)\end{bmatrix} &= -\left(C_k + a_k\begin{bmatrix}1 & 1\\ 1 & 1\end{bmatrix}\right)\begin{bmatrix}\delta x\left(t\right)\\ \delta y\left(t\right)\end{bmatrix} \\ &\quad + C_k\begin{bmatrix}\delta x(t-\tau)\\ \delta y(t-\tau)\end{bmatrix}\end{aligned} \tag{34}$$

where

$$C_k = \begin{bmatrix}\cos\left(\omega_k\tau\right) & \sin\left(\omega_k\tau\right)\\ -\sin\left(\omega_k\tau\right) & \cos\left(\omega_k\tau\right)\end{bmatrix}.$$

In order to obtain Eq. (34), we have used expressions (31) and (32). The characteristic equation is obtained from (34) by substituting $\delta x\left(t\right)=e^{\mu t}$

$$\det\left[\mu I + a_k^2\begin{bmatrix}1 & 1\\ 1 & 1\end{bmatrix} + C_k\left(1-e^{-i\mu\tau}\right)\right] = 0.$$

Finally, we obtain:

$$\begin{aligned}&\mu^2 + 2\mu\left(a_k^2 + \left(1-e^{-\mu\tau}\right)\cos\psi_\tau\right) \\ &+ 2a_k^2\left(1-e^{-\mu\tau}\right)\cos\psi_\tau + \left(1-e^{-\mu\tau}\right)^2 = 0,\end{aligned}$$

where $\psi_\tau=\omega_k\tau$.